npg

Bax and the mitochondrial permeability transition cooperate in the release of cytochrome *c* during endoplasmic reticulum-stress-induced apoptosis

D Zhang[1] and JS Armstrong*,[1]

Endoplasmic reticulum (ER) stress induces apoptosis by mechanisms that are not fully clear. Here we show that ER stress induced by the Ca^{2+}-ATPase inhibitor thapsigargin (THG) activates cytochrome *c*-dependent apoptosis through cooperation between Bax and the mitochondrial permeability transition (MPT) in human leukemic CEM cells. Pharmacological inhibition of the MPT as well as small interfering RNA (siRNA) knockdown of the MPT core component cyclophilin D blocked cytochrome *c* release and caspase-dependent apoptosis but did not prevent Bax activation, translocation or N-terminal exposure in mitochondria. siRNA knockdown of Bax also blocked THG-mediated cytochrome *c* release and apoptosis, but did not prevent MPT activation and resulted in caspase-independent cell death. Our results show that ER-stress-induced cell death involves a caspase and Bax-dependent pathway as well as a caspase-independent MPT-directed pathway.
Cell Death and Differentiation (2007) **14**, 703–715. doi:10.1038/sj.cdd.4402072; published online 15 December 2006

The endoplasmic reticulum (ER) regulates protein synthesis and intracellular calcium (Ca^{2+}) homeostasis. [1] Excessive ER stress can trigger apoptosis through a variety of mechanisms including redox imbalance, alterations in Ca^{2+} levels and activation of Bcl-2 family proteins.[2,3] Thapsigargin (THG), a sesquiterpenoid plant alkaloid, is frequently used to study the mechanisms regulating ER-stress-induced apoptosis and has previously been found to induce apoptosis in cancer cell lines via activation of the death receptor pathway and the mitochondrial pathway.[2,3]

The mitochondrial apoptotic signalling pathway involves activation of the proapoptotic Bcl-2 family member Bax, which induces permeabilization of the mitochondrial outer membrane and release of cytochrome *c*.[4–6] The mechanism(s) regulating Bax activation and translocation to mitochondria are incompletely understood, but its integration into the mitochondrial outer membrane appears to depend on a conformational change that exposes the N-terminus of the protein on the membrane surface, whereas its C-terminus facilitates membrane insertion.[7] In the outer membrane, Bax undergoes oligomerization to form a pore that facilitates the release of cytochrome *c*.[8,9] However, in addition to Bax, other key events are required to cause the complete release of cytochrome *c* from mitochondria including disruption of cytochrome *c* from the electron transport chain (ETC),[10,11] structural changes to the mitochondrial cristae inner membrane[12,13] and the activation of the mitochondrial permeability transition (MPT).[14,15]

The role of the MPT in apoptosis has recently been challenged by the observation that cells, isolated from genetically modified mice, lacking the MPT core component cyclophilin D (Cyp-D) were not protected from Bcl-2 family member regulated cell death suggesting that the MPT does not play a major role in apoptosis.[16,17] However, this idea contrasts previous reports showing that Bcl-2 family proteins, including Bax, interact with components of the MPT including the adenine nucleotide translocator (ANT) and the voltage-dependent anion channel (VDAC) to regulate apoptosis.[18–21] These controversies prompted us to investigate the role of the MPT and Bax in ER-stress-induced apoptosis.

In this study, we used small interfering RNA (siRNA) technology to investigate the role of the MPT and Bax in apoptosis induced by ER stress. Our results suggest that, in addition to Bax, calcium-dependent mitochondrial changes, including activation of the MPT, are crucial for the successful release of cytochrome *c* and induction of apoptosis by ER stress.

Results

THG treatment induces cytosolic and mitochondrial Ca^{2+} increase in CEM cells. Figure 1A shows results of an immunoblot for Cyp-D protein expression after transfection with control siRNA (left) and Cyp-D siRNA (right). Right lane shows ∼90% decrease in Cyp-D protein after transfection with Cyp-D siRNA compared to control. Figure 1B, left captions show FACS analysis histograms of Fluo3-AM-stained CEM cells before and after treatment with either THG±ruthenium 360 (Ru360), siRNA knockdown of Cyp-D or cyclosporin A (CsA). Thin black trace (control); heavy black trace (THG) and heavy green trace (a) THG+Ru360, (b) THG+Cyp-D siRNA treatment and (c)
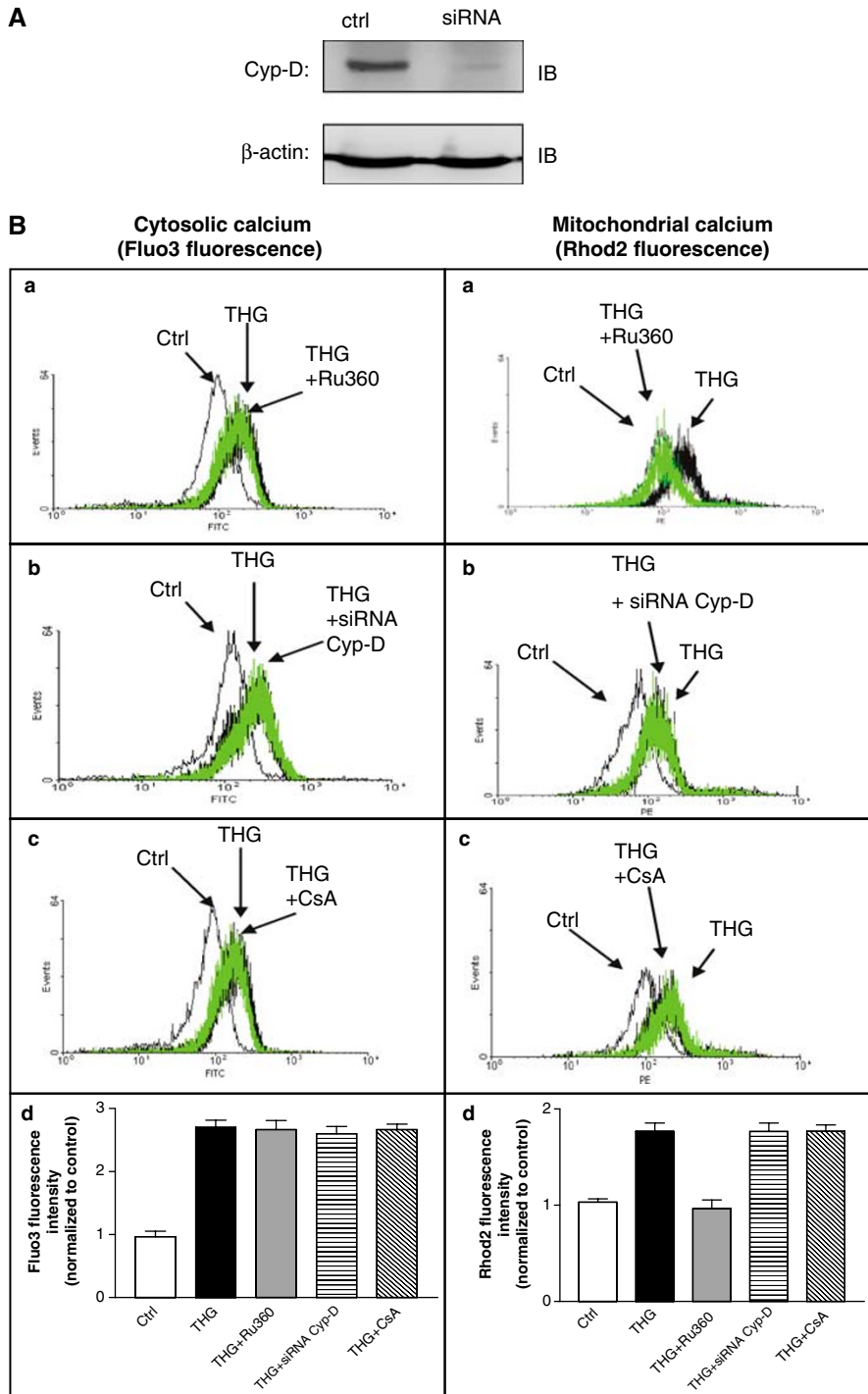
Figure 1 (**A**) Results of an immunoblot of Cyp-D protein expression in CEM cells after transfection with control siRNA (left) and Cyp-D siRNA (right) performed as described under 'Materials and Methods'. (**B**) *Cytosolic calcium panel:* representative FACS analysis histograms of Fluo3-AM-stained CEM cells treated with THG ± (a) Ru360, (b) Cyp-D siRNA and (c) CsA. Thin black trace: control; heavy black trace: THG; heavy green trace: THG + respective treatment. Panel d shows bar graph of cytosolic calcium levels (mean ± S.E) expressed as mean Fluo3 fluorescence intensity normalized to control. The cells were loaded with 1 μM Fluo3-AM for 15 min and the green fluorescence was immediately measured by flow cytometry using the FITC setting as described under 'Materials and Methods'. In each analysis, 10 000 events were recorded. *Mitochondrial calcium panel:* representative FACS analysis histograms of Rhod2-AM-stained CEM cells treated with THG ± (a) Ru360, (b) Cyp-D siRNA and (c) CsA. Thin black trace: control; heavy black trace: THG; heavy green trace: THG + respective treatment. Panel (d) shows bar graph of mitochondrial calcium levels (mean ± S.E) expressed as mean Rhod2 fluorescence intensity normalized to control. The cells were loaded with 250 nM Rhod 2-AM for 15 min and the red fluorescence was immediately measured by flow cytometry using the PE setting as described under 'Materials and Methods' In each analysis, 10 000 events were recorded. (**C**) Figure shows representative confocal images of CEM cells loaded with DAPI, MitoTracker green and Rhod2-AM after treatment with THG or THG + Ru360 as described in the Materials and Methods section
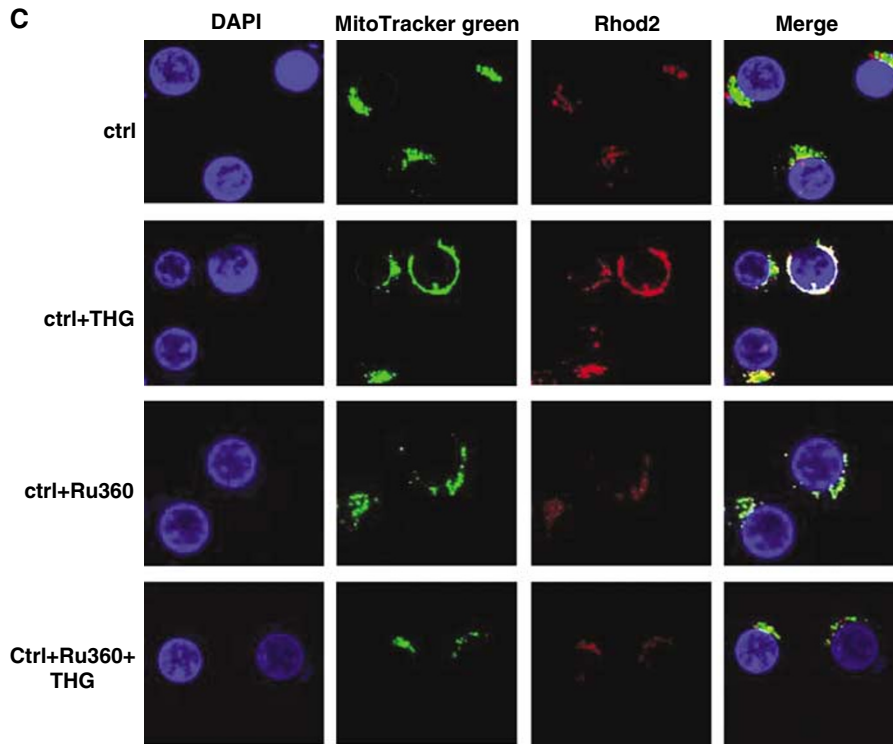
Figure 1 (*Continued*)

THG + CsA. Figure shows a representative example of three independent experiments. In each analysis, 10 000 events were recorded. Figure 1B, left caption (d) shows a bar graph of cytosolic calcium levels expressed as mean Fluo3 fluorescence intensity normalized to control. The data are expressed as means ± S.E. ($n = 3$). Results show that THG significantly increased Fluo3 fluorescence in CEM cells, which was not altered by either treatment with Ru360 (to block mitochondrial calcium uptake), by MPT inhibition with CsA or by siRNA Cyp-D knockdown. Figure 1B, right captions show FACS analysis histograms of Rhod2-AM-stained CEM cells as described above for Fluo3-AM. Figure 1B, right caption (d) shows a bar graph of mitochondrial calcium levels expressed as mean Rhod2 fluorescence intensity normalized to control as described above for Fluo3. Results show that THG significantly increased Rhod2 fluorescence in CEM cells, which was effectively blocked by treatment with Ru360, but not by MPT inhibition with CsA or by siRNA Cyp-D knockdown. Figure 1C shows representative confocal images of CEM cells loaded with 4'-6-diamidino-2-phenylindole (DAPI), MitoTracker green and Rhod2-AM and then treated with THG or THG + Ru360. Merge shows that THG increased Rhod2 fluorescence in mitochondria of CEM cells that was blocked by Ru360. Results support those obtained by FACS analysis.

THG causes loss of mitochondrial membrane potential ($\Delta_{\Psi m}$): evidence of Ca^{2+}-induced MPT. $\Delta_{\Psi m}$ was determined by monitoring the fluorescence of the cationic potentiometric dye TMRM performed as described in the

Materials and Methods section. Figure 2 shows representative two-dimensional colour density plots of TMRM-stained cells showing percentage numbers of cells with intact $\Delta_{\Psi m}$ (TMRM fluorescence in top right quadrant) *versus* percentage number of cells with reduced $\Delta_{\Psi m}$ (TMRM fluorescence in bottom left quadrant). Figure shows TMRM fluorescence of cells treated for 36 h with (a) RPMI (control), (b) THG, (c) THG + Ru360, (d) THG + siRNA Cyp-D and (e) THG + CsA. The figure shows a representative example of three independent experiments. In each analysis, 10 000 events were recorded. Percentage cells with TMRM fluorescence at 36 h: (a) control ∼93%, (b) THG ∼8%, (c) THG + Ru360 ∼53%, (d) THG after siRNA Cyp-D knockdown ∼59% and (e) THG + CsA ∼68%. Figure 2f shows the percentage (mean ± S.E.) of CEM cells with intact $\Delta_{\Psi m}$ at 0, 12, 24 and 36 h after treatment with THG as described above and shows that THG induced a time-dependent loss of TMRM fluorescence over 36 h which was significantly blocked by Ru360, CsA and by siRNA Cyp-D knockdown.

THG induces mitochondrial cytochrome *c* release, caspase-3 cleavage and DNA fragmentation of CEM cells. Figure 3A shows representative results of cytochrome *c* immunoblots after cells were co-incubated with THG + Ru360 (top panel), THG + siRNA Cyp-D (middle panel) or THG + CsA (bottom panel). β-Actin was used as a loading control. Results show that THG induced a time-dependent increase in cytosolic cytochrome *c* band, which was significantly reduced by each of the treatments
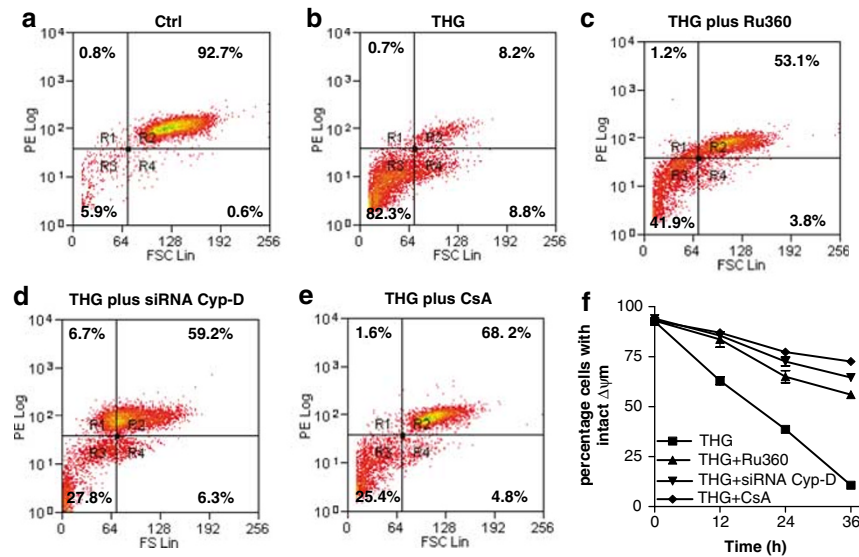
Figure 2 Representative TMRM fluorescence two-dimensional colour density plots showing percentage number of cells with intact $\Delta_{\Psi m}$ (TMRM fluorescence in top right quadrant) and percentage number of cells with reduced $\Delta_{\Psi m}$ (TMRM fluorescence in bottom left quadrant) 36 h after treatment with THG. (**a**) RPMI (control), (**b**) THG, (**c**) THG + Ru360, (**d**) THG + siRNA CyD and (**e**) THG + CsA. The cells were loaded with 250 nM TMRM for 15 min and the red fluorescence was immediately measured by flow cytometry using the PE setting as described under 'Materials and Methods'. In each analysis, 10 000 events were recorded. Panel (**f**) shows a graph of the percentage (mean ± S.E.) of CEM cells with intact $\Delta_{\Psi m}$ determined at 0, 12, 24 and 36 h after treatment with THG as described above

described above. Figure 3B shows a bar graph of mean caspase-3 activity 36 h after cells were treated with THG ± Ru360, Cyp-D siRNA or CsA. Results show that each treatment significantly inhibited caspase-3 processing. Figure 3C shows representative cell cycle analysis FACS histograms of propidium iodide (PI)-stained CEM cells after treatment with (a) RPMI (control), (b) THG, (c) THG + Ru360, (d) THG + siRNA Cyp-D and (e) THG + CsA for 36 h. Inset figures show results of DAPI staining of cells shown in corresponding FACS histograms. Results show that inhibition of mitochondrial Ca^{2+} increase or MPT activation blocked induction of apoptosis.

CsA blocks THG-induced cell death in siRNA Cyp-D knockdown cells. To investigate whether CsA was nonspecifically (not by its effects on the MPT) blocking THG-induced cell death, we treated siRNA Cyp-D knockdown cells for 48 h with THG in the presence and absence of CsA. Figure 4A shows that CsA blocked THG-induced loss of cell viability in siRNA Cyp-D knockdown cells. These results indicated that THG-mediated release of cytochrome *c* from the mitochondria of CEM cells involved the MPT as well as a non-MPT pathway. Figure 4B shows electron micrographs (EM) of the mitochondrial ultrastructure of CEM cells after treatment with (a) RPMI control, (b) THG and (c) THG + CsA for 36 h. Results show that CsA preserved the ultrastructure of the mitochondrial cristae (indicated by arrow heads).

Bax translocation and N-terminal exposure is independent of MPT. As Bax is known to regulate cytochrome *c* release and cell death, we next investigated the role of Bax in THG-induced cell death. Figure 5A shows representative Bax (N20 antibody) immunoblots performed on the mitochondrial fractions taken from CEM cells treated with (top panel) THG ± Ru360, (middle panel) THG ± siRNA Cyp-D and (bottom panel) THG ± CsA for 24 h. Manganese superoxide dismutase (MnSOD) was used as a loading control. Results show that THG caused a time-dependent increase in mitochondrial Bax which, was not significantly altered by each of the treatments described above, indicating that Bax activation and translocation to mitochondria was independent of the MPT. We next treated CEM cells with THG ± the Ca^{2+} chelating agent BAPTA-AM to determine the role of cytosolic Ca^{2+} in Bax activation. Figure 5B (part a) shows representative Fluo3-AM FACS analysis histograms as described in Figure 1. Thin black trace ∼ control; heavy black trace ∼ THG and heavy green trace THG + BAPTA-AM. Figure 5B, (part b) shows bar graph of cytosolic calcium levels ± BAPTA-AM expressed as mean Fluo3 fluorescence intensity normalized to control as described in Figure 1. The results show that BAPTA-AM blocked cytosolic Ca^{2+} increase. Figure 5B (part c) shows Bax immunoblot after treatment of cells with THG ± BAPTA-AM for 24 h as described in Figure 5A showing that Bax activation and translocation to mitochondria was not significantly altered by BAPTA-AM. These results indicated that Bax activation was independent of THG-induced cytosolic Ca^{2+} increase and MPT.

siRNA Bax knockdown blocks THG-induced release of cytochrome *c* and leads to caspase-independent cell death. Figure 6A shows results of an immunoblot for Bax protein expression after transfection with control siRNA (left) and Bax siRNA (right). Right lane shows ∼90% decrease in Bax protein after transfection with Cyp-D siRNA compared to control. Figure 6B shows (a) representative FACS analysis histograms of Fluo3-AM-stained CEM cells ± THG before
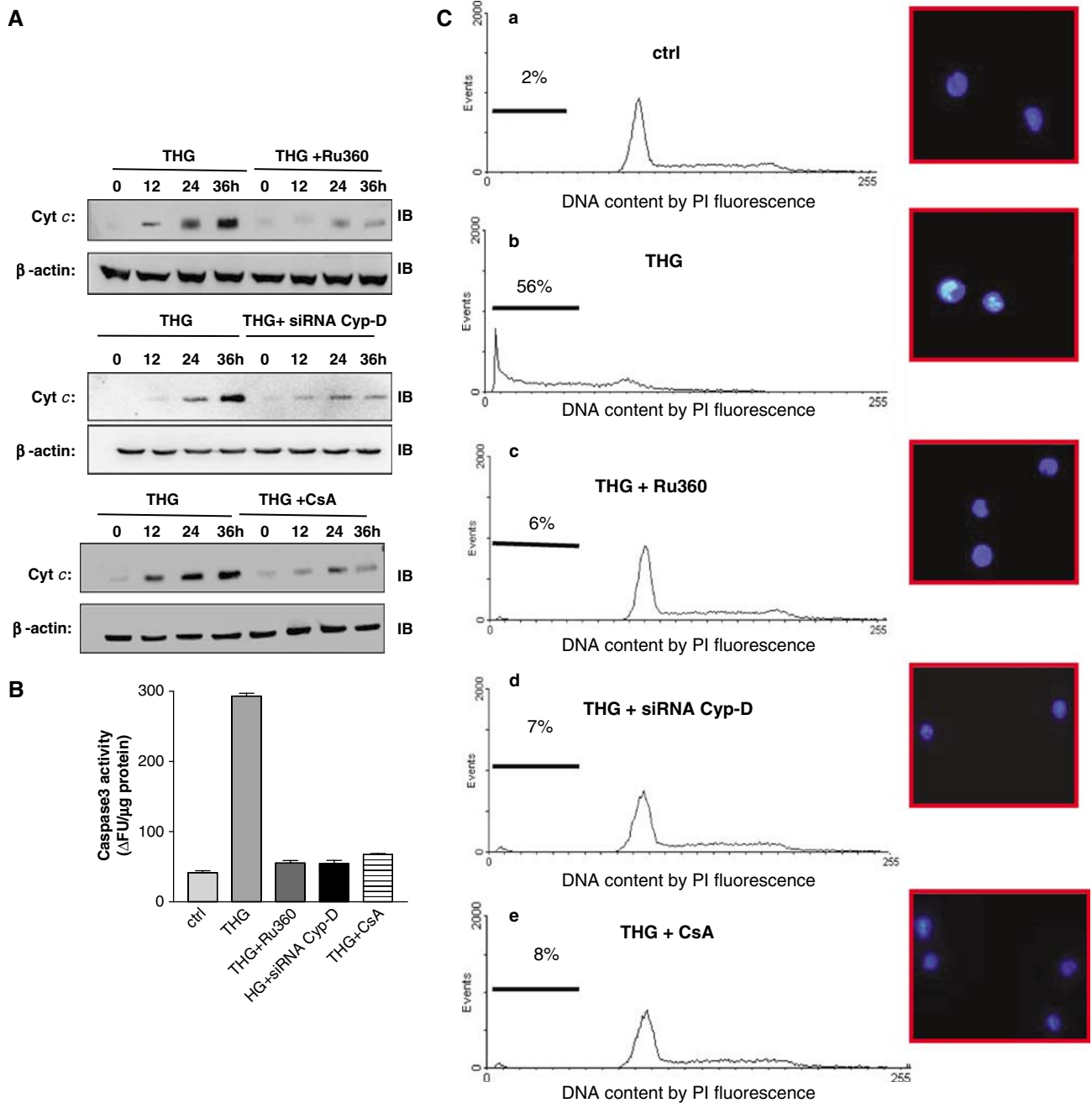
A

B

C

Figure 3 (**A**) Top panel shows representative cytochrome *c* immunoblot determined on the cytosolic fractions of CEM cells before and after treatment with THG ± Ru360 for 0, 12, 24 and 36 h. β-Actin was used as a loading control. Middle panel shows representative cytochrome *c* immunoblot determined on the cytosolic fractions of CEM cells after treatment with THG for 0, 12, 24 and 36 h before and after Cyp-D siRNA knockdown. β-Actin was used as a loading control. Bottom panel shows representative cytochrome *c* immunoblot determined on the cytosolic fractions of CEM cells before and after treatment with THG ± CsA for 0, 12, 24 and 36 h. β-Actin was used as a loading control. (**B**) Figure shows bar graph of caspase-3 activity (mean ± S.E.) before and after treatment with THG ± Ru360; THG ± CsA or THG before and after treatment with Cyp-D siRNA for 36 h determined as described under 'Methods and Materials'. (**C**) Representative cell cycle analysis FACS histograms of PI-stained CEM cells after treatment with (a) RPMI (control), (b) THG, (c) THG + Ru360, (d) THG after pretreatment with Cyp-D siRNA and (e) THG + CsA for 36 h. Percentage cells containing hypodiploid amount of DNA (sub-G1 fraction) indicated. Inset figures show results of DAPI staining of cells shown in corresponding FACS histograms

and after siRNA Bax knockdown: black trace: parental control; green trace: siRNA Bax. (b) Bar graph of cytosolic calcium levels (mean ± S.E) expressed as mean Fluo3 fluorescence intensity normalized to control. (c) Representative FACS analysis histograms of Rhod2-AM-stained CEM cells ± THG before and after siRNA Bax

knockdown: black traces ~ *parental cells*: control, THG and THG + Ru360; green traces ~ *siRNA Bax knockdown cells*: control, THG and THG + Ru360. (d) Bar graph of mitochondrial calcium levels (mean ± S.E) expressed as mean Rhod2 fluorescence intensity normalized to control. Figure 6C shows a representative cytochrome *c* immunoblot
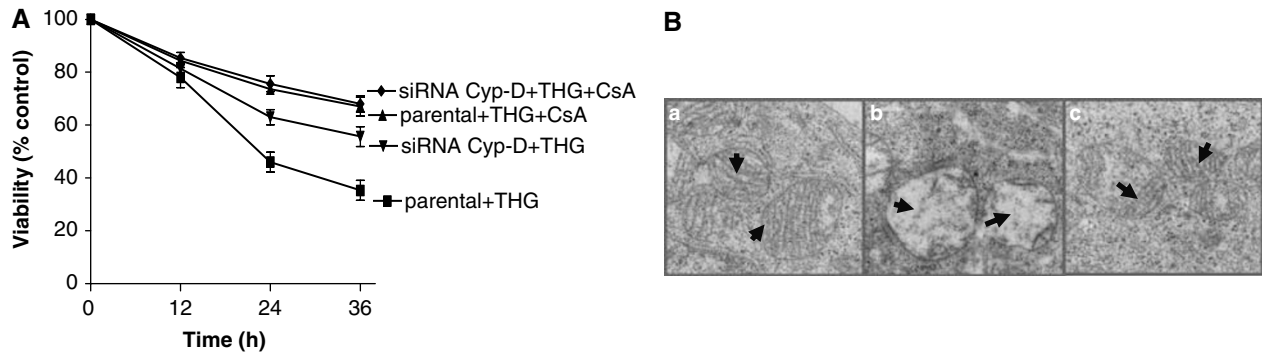
Figure 4 (**A**) Parental CEM cells and Cyp-D knockdown cells were treated with THG ± CsA and cell viability was determined by trypan blue exclusion at 0, 12, 24 and 36 h. (**B**) Mitochondrial ultrastructure of CEM cell mitochondria determined by TEM before and after treatment with THG ± CsA for 36 h. (a) RPMI control, (b) THG and (c) THG + CsA (arrowheads point to mitochondrial internal cristae structure)
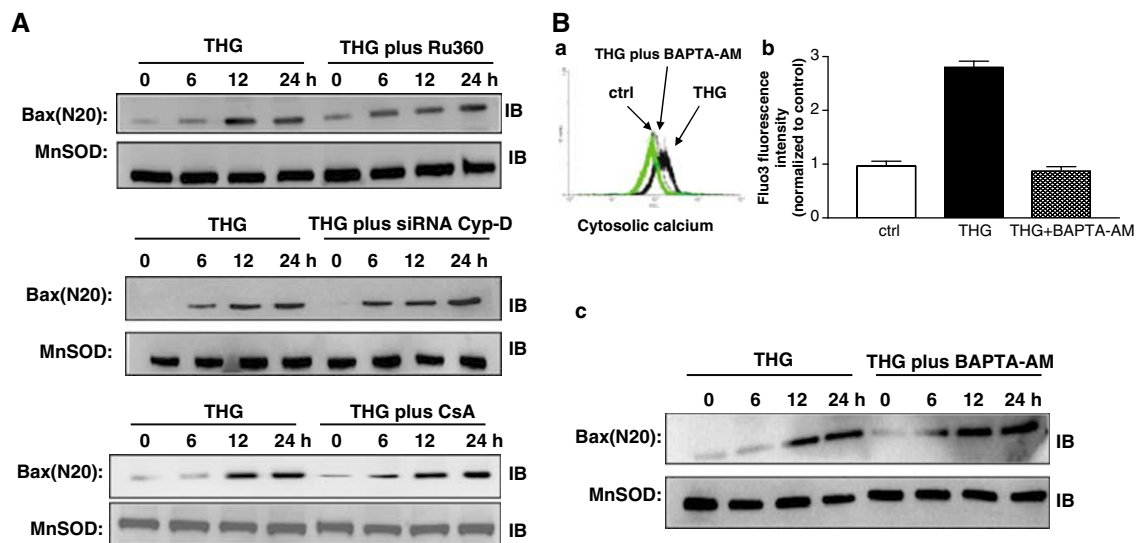

Figure 5 (**A**) Top panel shows representative Bax (N20 antibody) immunoblot determined on the mitochondrial fractions of CEM cells before and after treatment with THG ± Ru360 for 0, 6, 12 and 24 h. MnSOD was used as a loading control. Middle panel shows representative Bax (N20 antibody) immunoblot determined on the mitochondrial fractions of CEM cells treated with THG for 0, 6, 12 and 24 h before and after pretreatment with Cyp-D siRNA. MnSOD was used as a loading control. Bottom panel shows representative Bax (N20 antibody) immunoblot determined on the mitochondrial fractions of CEM cells before and after treatment with THG ± CsA for 0, 6, 12 and 24 h. MnSOD was used as a loading control. (**B**): (a) Representative FACS analysis histograms of Fluo3-AM-stained CEM cells after treatment with THG ± BAPTA-AM (determined as described in Figure 1B). Thin black trace shows control cells; heavy black trace shows cells after treatment with THG and heavy green trace shows cells after treatment with THG + BAPTA-AM. (b) Bar graph showing cytosolic calcium levels in the presence and absence of BAPTA-AM expressed as mean Fluo3 fluorescence intensity normalized to control. The data are expressed as means ± S.E. ($n = 3$). (c) Shows representative Bax (N20 antibody) immunoblot determined on the mitochondrial fractions of CEM cells before and after treatment with BAPTA-AM for 0, 6, 12 and 24 h. MnSOD was used as a loading control

Figure 6 (**A**) results of an immunoblot of Bax (N-20 antibody) protein expression performed on CEM cells after transfection with either control siRNA or Bax siRNA. (**B**): (a) Representative FACS analysis histogram of Fluo3-AM-stained CEM cells before and after siRNA Bax knockdown in the presence and absence of THG. Black trace: parental control cells ± THG; green trace: siRNA Bax ± THG. (b) Bar graph of cytosolic calcium levels in CEM cells after treatment with THG before and after siRNA Bax knockdown (mean ± S.E.) expressed as mean Fluo3 fluorescence intensity normalized to control. (c) Representative FACS analysis histograms of Rhod2-AM-stained CEM cells before and after siRNA Bax knockdown in the presence and absence of THG ± Ru360. Black trace: parental control cells, parental control cells + THG and parental control cells + THG + Ru360; green trace: siRNA Bax control, siRNA Bax + THG and siRNA Bax + THG + Ru360. (d) Bar graph of mitochondrial calcium levels in CEM cells before and after siRNA Bax knockdown in the presence and absence of THG or THG + Ru360 (mean ± S.E) expressed as mean Rhod2 fluorescence intensity normalized to control. (**C**) Representative cytochrome *c* immunoblot determined on the cytosolic fractions of CEM cells treated with THG for 0, 12, 24 and 36 h before and after siRNA Bax knockdown. β-Actin was used as a loading control. (**D**) Representative TMRM fluorescence two-dimensional colour density plots showing percentage number of cells with intact $\Delta_{\Psi m}$ and percentage number of cells with reduced $\Delta_{\Psi m}$ before and after treatment with THG for 48 h (as described in Figure 2). (a) Parental CEM cells + THG, (b) Parental CEM cells + THG + zVADfmk, (c) siRNA Bax knockdown CEM cells + THG, (d) siRNA Bax knockdown CEM cells + THG + zVADfmk, (e) siRNA Bax knockdown CEM cells + THG + CsA. The cells were loaded with 250 nM TMRM for 15 min and the red fluorescence was immediately measured by flow cytometry using the PE setting as described under 'Materials and Methods' In each analysis, 10 000 events were recorded. Inset figure (f) shows a graph of the percentage (mean ± S.E.) of CEM parental and siRNA Bax knockdown cells with intact $\Delta_{\Psi m}$ determined at 0, 24 and 48 h after treatment with THG as described above. (**E**) Graph showing viability of CEM parental and siRNA Bax knockdown cells after treatment with THG ± zVADfmk and siRNA Bax knockdown cells + CsA for 0, 24, 48, 72 and 96 h assayed by trypan blue exclusion. (**F**) Representative FACS analysis cell cycle histograms of PI-stained CEM parental and siRNA Bax knockdown CEM cells after treatment with THG for 0, 24, 48, 72 and 96 h. Percentage cells containing hypodiploid amount of DNA (sub-G1 fraction) indicated. (**G**) Bar graph of caspase-3 activity after treatment of CEM parental and siRNA Bax knockdown CEM cells with THG for 0, 12, 24, 36 and 48 h

determined on cytosolic fractions taken from CEM parental cells and CEM siRNA Bax knockdown cells after treatment with THG every 12 h for a total of 36 h. Results show that cytosolic cytochrome *c* protein band was blocked by siRNA Bax knockdown. Figure 6D, $\Delta_{\Psi m}$ was determined in parental cells treated with THG±zVADfmk and siRNA Bax

knockdown cells treated with THG±zVADfmk or CsA by monitoring TMRM fluorescence as described for Figure 2. Figure shows TMRM fluorescence of cells monitored at 0, 24 and 48 h treated with (a) THG, (b) THG+zVADfmk, (c) THG+siRNA Bax, (d) THG+siRNA Bax+zVADfmk and (e) THG+siRNA Bax+CsA. After 48 h treatment of CEM
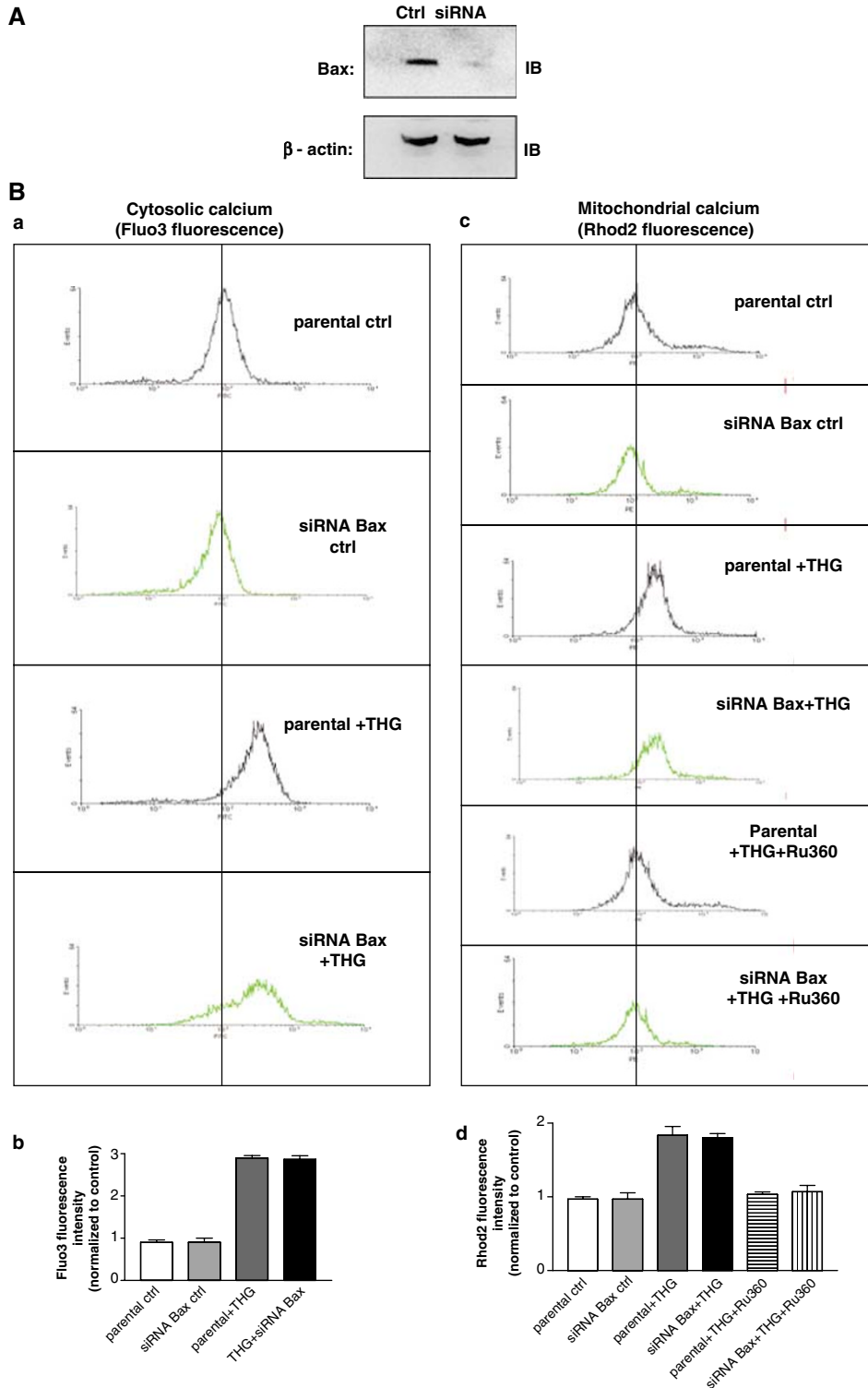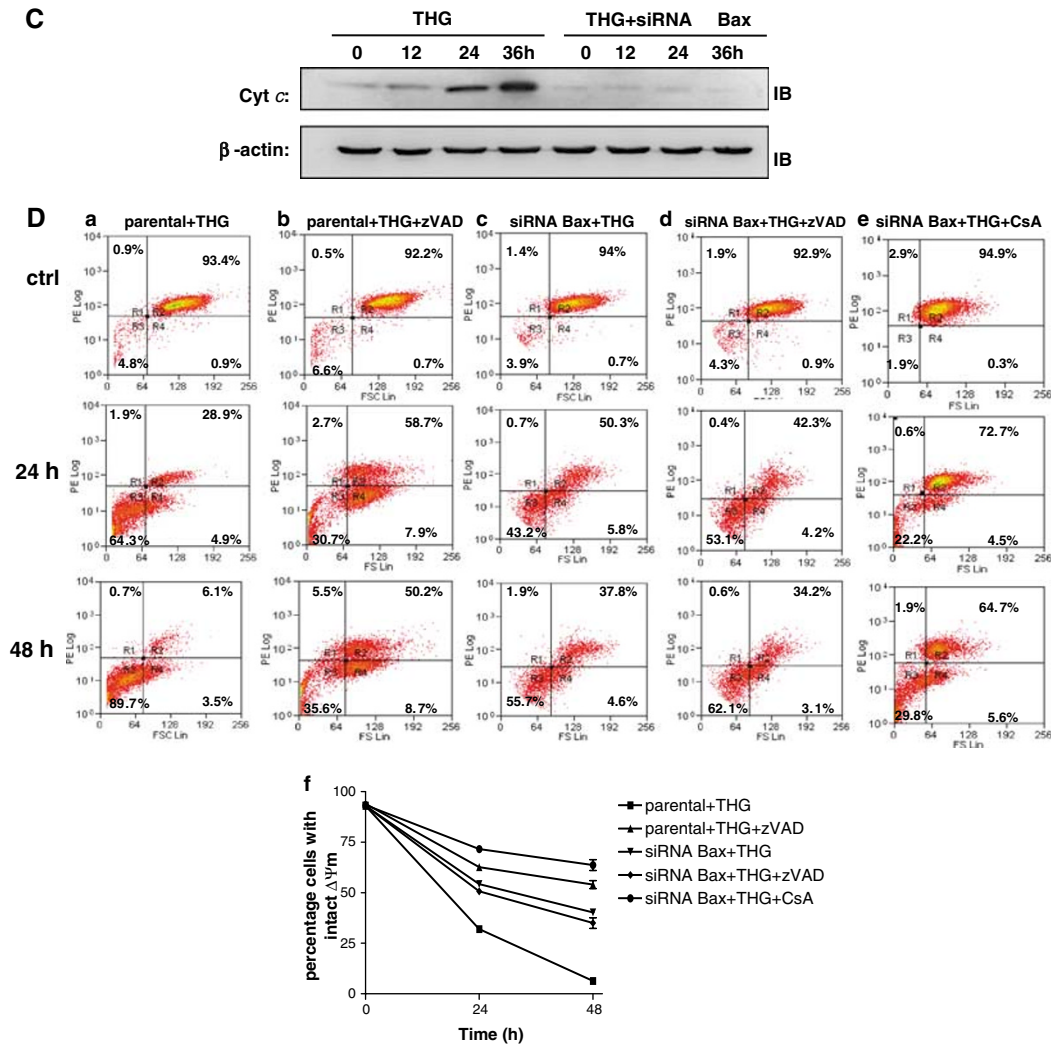
Figure 6 (*Continued*)

parental cells with THG, loss of TMRM fluorescence (lower left quadrant of colour density plot) occurred in *panel a* ~ 90% of cell population compared to 36% in cells treated with THG + zVADfmk, *panel b*. After 48 h treatment of siRNA Bax knockdown cells with THG, loss of TMRM fluorescence occurred, in *panel c* ~ 56% of cell population compared to ~ 62% in cells treated with zVADfmk as showed in *panel d*, whereas treatment with CsA caused loss of TMRM fluorescence in ~ 30% of cell population, *panel e*. Results show that THG-induced loss of $\Delta_{\Psi m}$ in parental cells was blocked by caspase inhibition, whereas loss of $\Delta_{\Psi m}$ in siRNA Bax knockdown cells was not blocked by caspase inhibition, but was significantly protected by CsA. Figure 6D, (f) shows the percentage (mean ± S.E.) of CEM cells with intact $\Delta_{\Psi m}$. Figure 6E shows viability of THG-treated parental cells and siRNA Bax knockdown cells in the presence and absence of zVADfmk. Results show that zVADfmk blocked loss of cell viability induced by THG in parental cells, but not in siRNA Bax knockdown cells. Figure 6F shows representative FACS analysis cell cycle histograms of PI-stained, THG-treated CEM parental cells and siRNA Bax knockdown cells

monitored at 0, 24, 48, 72 and 96 h. Results show that THG treatment induced a significant increase in the subG1 fraction of parental CEM cells but not in siRNA Bax knockdown CEM cells. Figure 6G shows a bar graph of caspase-3 activity at 0, 12, 24, 36 and 48 h determined as described for Figure 3B. Results show that siRNA Bax knockdown inhibited THG-mediated caspase-3 processing. Together, these results indicated that in the absence of Bax, THG-induced cell death is caspase independent.

Contribution of the MPT to the release of cytochrome *c* from mitochondria. During ER-stress-induced apoptosis, we observed that Bax was necessary but not sufficient for complete cytochrome *c* release from mitochondria. We, therefore, considered that the MPT was involved in the mobilization of cytochrome *c* from mitochondria and Bax provided a cytochrome *c* access channel to the cytosol. To investigate the role of the MPT in the release of cytochrome *c* release, we treated isolated rat liver mitochondria (RLM) with either Ca^{2+} to induce the MPT or Ca^{2+} + CsA to block the MPT and determined the relative amount of cytochrome *c*
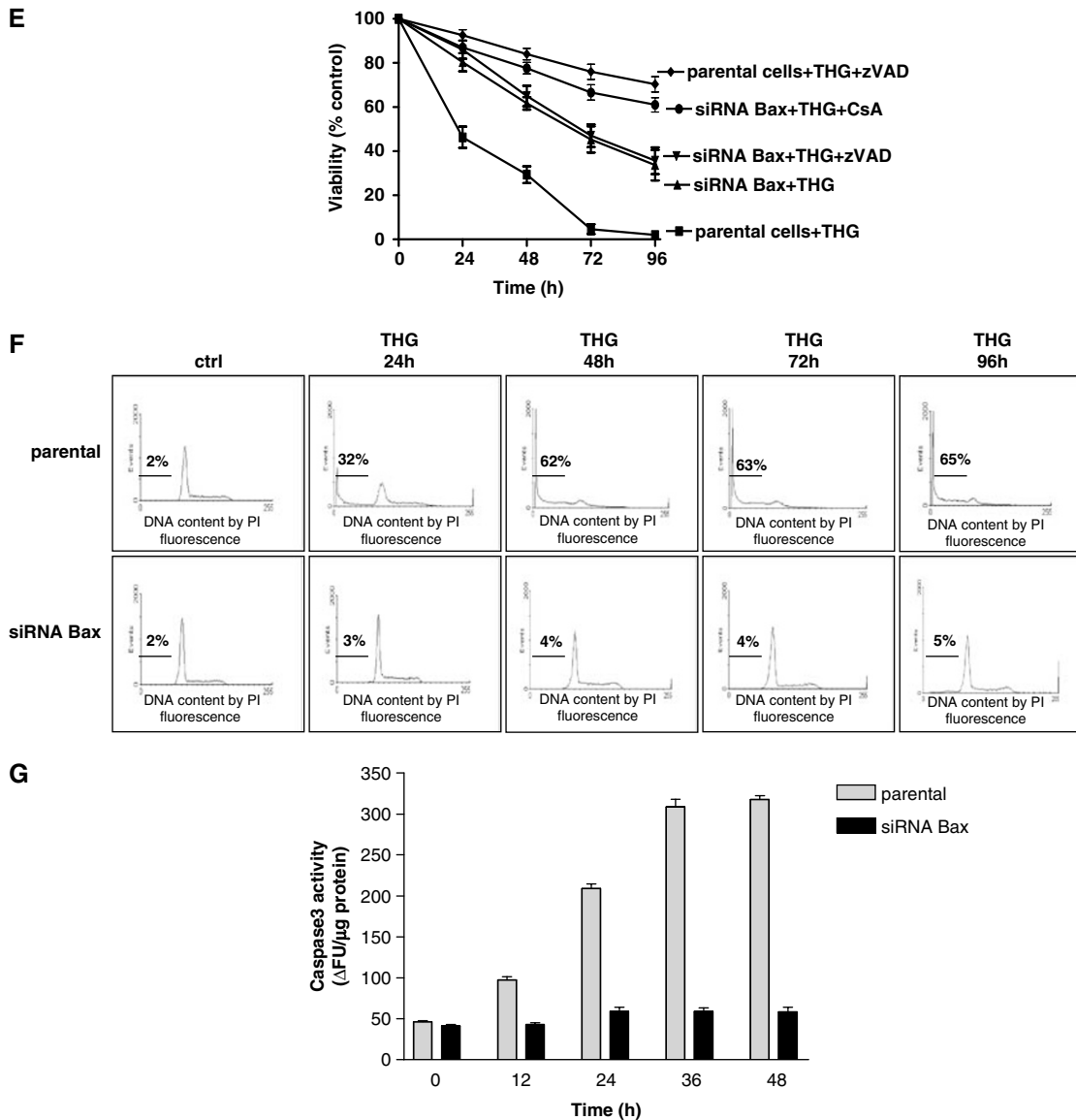
E

F

G

Figure 6 (*Continued*)

released into the mitochondrial suspension buffer by Western blot. To investigate the role of Bax as a pore-forming protein in the mitochondrial outer membrane, we determined the proportion of cytochrome *c* in the mitochondrial inter-membrane space by removing the mitochondrial outer membrane of RLM with digitonin (DIG) and determining cytochrome *c* release into the mitochondrial suspension buffer by Western blot. Figure 7A shows a representative example of Ca^{2+}-induced swelling profile of RLM in the presence and absence of CsA showing that CsA blocks large amplitude swelling indicative of the MPT. Figure 7B top panel shows oxygen consumption and calculated respiratory control ratios (RCR) of RLM suspensions (a) before and (b) after treatment with DIG; middle panel shows representative results of an immunoblot for cytochrome *c* performed on aliquots of mitochondrial suspension buffer (a) after treatment with $Ca^{2+} \pm CsA$ and (b) after treatment with either Ca^{2+} or DIG (see Materials and Methods); bottom panel shows bar graph of relative cytochrome *c* band density determined from the immunoblots shown in 'middle panel' measured by scanning densitometry. Results show that the major fraction of cytochrome *c* is released upon MPT activation and a minor fraction is released by removing the mitochondrial outer membrane. In conjunction with our *in situ* data, these results suggest that the Bax-mediated permeabilization of the outer mitochondrial membrane provides the critical access point for cytochrome *c* release to the cytosol during ER-stress-induced apoptosis, but requires the MPT- and non-MPT-mediated structural changes to cristae for complete release of cytochrome *c* and activation of apoptosis. However, this is not to say that ER-stress-induced activation of Bax only causes outer
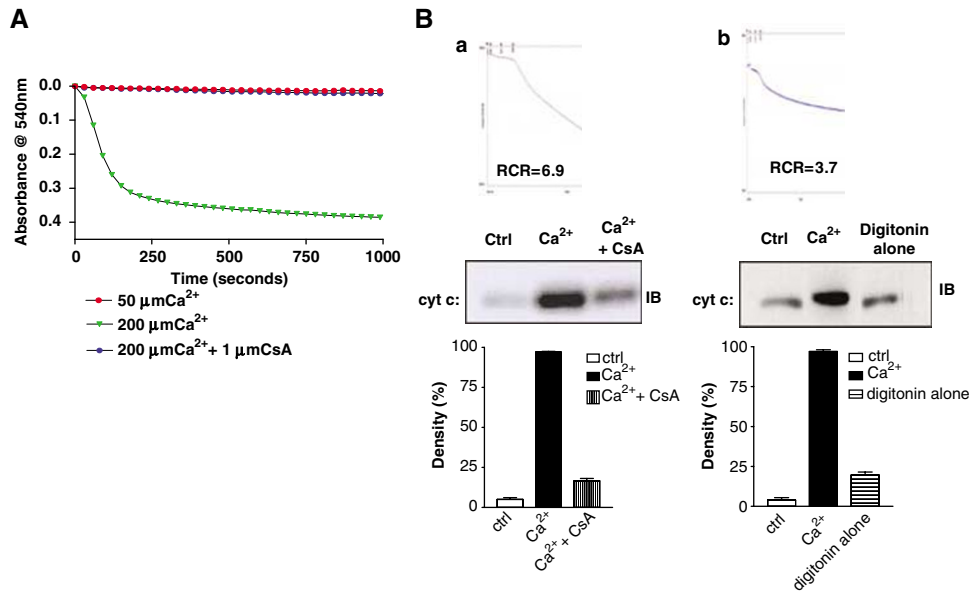
Figure 7 (**A**) The figure shows representative example of Ca^{2+}-induced swelling profile of RLM in the presence and absence of CsA. RLM (0.5 mg protein/ml) were treated with 200 μM Ca^{2+} $\pm$ CsA and absorbance at 540 nm was monitored as described under 'Materials and Methods'. (**B**) Top panel: (a) Oxygen consumption of isolated RLM with estimated RCR $\sim$ 6.9, (b) oxygen consumption of RLM after treatment with DIG with estimated RCR $\sim$ 3.7. Middle panel: (a) representative cytochrome *c* immunoblot determined on the supernatant fractions taken from RLM suspensions treated with Ca^{2+} $\pm$ CsA. (b) Representative cytochrome *c* immunoblot determined on the supernatant fractions taken from RLM suspensions treated with Ca^{2+} or DIG. Bottom panel shows bar graph of cytochrome *c* band density determined from the immunoblots shown in 'middle panel' measured by scanning densitometry

membrane permeabilization, as it may also be involved in facilitating mitochondrial inner membrane changes which have not been investigated here.

Discussion

In this study, we investigated mitochondrial events regulating ER-stress-induced apoptosis in human leukemic CEM cells using the drug THG. Three independent lines of evidence showed a key role for increased mitochondrial Ca^{2+} in THG-mediated cytochrome *c* release and induction of apoptosis: (1) pharmacological inhibition of mitochondrial Ca^{2+} increase (using Ru360 to block uniporter function), (2) CsA, the classical MPT inhibitor and (3) siRNA knockdown of Cyp-D all blocked cytochrome *c* release and induction of apoptosis. These results indicated that increased mitochondrial Ca^{2+} levels and MPT activation were required for the induction of CEM cell death. However, as CsA is relatively nonspecific in its action, we also considered that, in addition to its effects on the MPT, CsA might be inhibiting apoptosis via an additional mechanism.[22–26] To determine the role of CsA in the regulation of THG-induced apoptosis, we treated siRNA Cyp-D knockdown CEM cells with THG in the presence and absence of CsA (Figure 4). We found that CsA protected CEM cells from THG-induced loss of viability even in the absence of Cyp-D, which indicated that in addition to its known effects on the MPT, CsA was protecting CEM cells against ER-stress-induced apoptosis by an additional mechanism. Although, the nature of this protective mechanism is unclear, EM results showed that CsA preserved the mitochondrial cristae structure. In agreement with this idea, previous findings of Scorrano *et al.*[12] showed that mitochondrial cytochrome *c* release, in this case induced by Bid, also involved a CsA-sensitive structural remodelling of mitochondrial cristae.

THG-induced ER stress also caused the robust activation, translocation and N-terminal exposure of Bax in the mitochondria of CEM cells. The mechanism involved is currently unknown, but may involve the death receptor pathway via CHOP, DR5 and caspase-8 as previously reported,[3] as we found that Bax translocation to mitochondria was not dependent on ER-stress-induced Ca^{2+} increase (Figure 5B, part c). The role of Bax in THG-induced apoptosis in CEM cells was investigated using siRNA to knockdown Bax protein expression. siRNA knockdown of Bax completely prevented THG-induced cytochrome *c* release and partially inhibited apoptosis, indicating that Bax was required for the induction of cytochrome *c*-dependent apoptosis. However, Bax activation was unimpaired by either Ru360, CsA or Cyp-D knockdown, indicating that Bax alone was insufficient for successful induction of apoptosis during ER stress. This suggested that Bax and the MPT were independent signals that cooperated during ER-stress-induced apoptosis in CEM cells. Our results contrast a recent report which showed that the MPT signalled the activation and translocation of Bax to mitochondria during TMRM-induced photoexcitation.[27] Although the reason for this discrepancy is not known, as the MPT can be either CsA-regulated or CsA-unregulated,[28–31] the photoexitation model might represent the unregulated MPT resulting from excessive free radical-induced redox stress which has previously been found to activate Bax.[32–34]

To investigate the relative contribution of Bax and the MPT to cytochrome *c* release in CEM cells, we noted that after MPT inhibition a minor fraction of cytochrome *c* (estimated at between 15 and 20%) was detected by immunoblot. We

considered that this minor fraction, which was insufficient to activate apoptosis, might represent the cytochrome *c* residing in the mitochondrial inter-membrane space and not functioning in electron transport. To investigate this, we considered that we should be able to measure a similar quantity of cytochrome *c* released from the inter-membrane space of isolated RLM after removing the mitochondrial outer membrane, and if this fraction of cytochrome *c* was not involved in electron transport, then the mitochondria would remain coupled. Figure 6B shows that after treatment with the detergent DIG to remove the outer mitochondrial membrane, RLM released approximately ∼15–20% of their total complement of cytochrome *c* into the mitochondrial suspension buffer, but still remained significantly coupled (although RCR fell from 6.9 to 3.7). These studies provided evidence, although indirect, that during ER-stress-induced apoptosis, the MPT was responsible for the release of a major fraction of cytochrome *c* derived from the mitochondrial ETC. As we also found that CsA blocked the release of approximately 80–85% of cytochrome *c* from isolated RLM treated with Ca^{2+} to induce the MPT (Figure 7B (a) middle panel), this also supported the notion that the MPT was responsible for the release of the major fraction of cytochrome *c* from RLM. These results support the idea that Bax forms a simple pore allowing cytochrome *c* release into the cytosol as previously reported,[35] and indicate that the MPT as well as structural changes occurring in the mitochondrial cristae are essential for the complete release of cytochrome *c* during ER-stress-induced apoptosis (this idea is shown in Figure 8).
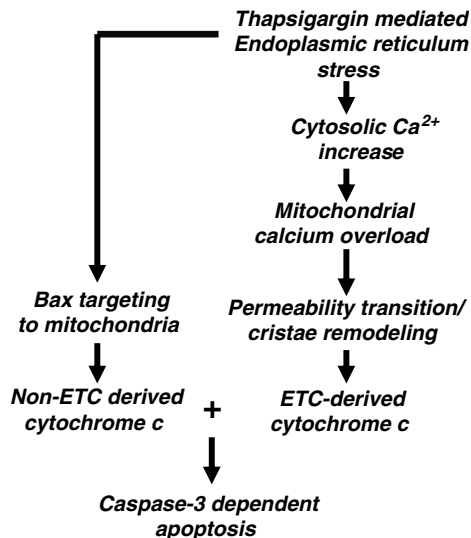
In conclusion, our results show that ER-stress-induced apoptosis requires cooperation between Bax and Ca^{2+}-dependent mitochondrial changes including the MPT and CsA-sensitive structural changes to mitochondrial cristae. The result of this cooperation is a coordinated mechanism that regulates the complete release of mitochondrial cytochrome *c* and activation of the mitochondrial death pathway.

Materials and Methods

Materials and cell culture. Chemicals including THG and BAPTA-AM were obtained from Molecular Probes (Eugene, OR, USA). Ru360 was purchased from Calbiochem (San Diego, CA, USA). Fluorescent probes including tetra-methyl rhodamine methyl ester (TMRM), Fluo3-AM, Rhod2-AM, MitoTracker green, PI and 4′,6-diamidino-2-phenylindole, dihydrochloride (DAPI) were from Molecular Probes (Eugene, OR, USA). zVADfmk and DEVDfmk caspase inhibitors and CsA were purchased from Sigma Chemical Company.(St. Louis, MO, USA) CEM cells were passaged daily to maintain them in log-phase growth and kept at a nominal concentration of $2.5–5 \times 10^5$/ml. Cell viability studies were performed by trypan blue exclusion method.

Apoptosis determination. THG was used at a concentration of 1 μM unless otherwise stated. Cellular apoptosis was determined by performing FACS cell cycle analysis of PI (20 μg/ml)-stained CEM cells. The percentage of cells in the sub-G1 zone was taken to indicate the percentage of cells undergoing apoptosis. DAPI (3 μM) staining was also monitored by fluorescence microscopy to visually estimate cells containing fragmented DNA.

Caspase- 3 activity assays. EnzChek®Caspase-3 Assay kits were purchased from Molecular probes (Eugene, OR, USA). CEM cell caspase-3 activity was determined using a caspase-3 synthetic fluorescent substrate. Assays were performed according to the manufacturer's instructions. Substrate cleavage increases fluorescence, which was measured using Molecular Probes fluorometer model # GEMINI XS (excitation at 342 nm and emission at 441 nm).

FACS analysis for cytosolic and mitochondrial Ca^{2+} levels. Cytosolic Ca^{2+} levels were determined using the fluorescent dye Fluo3-AM (1 μM) (log mode in FITC setting). Mitochondrial Ca^{2+} levels were determined using the fluorescent dye Rhod2-AM (250 nM) (log mode PE setting). Cells (parental, siRNA Cyp-D knockdown and siRNA Bax knockdown) were treated with THG ± Ru360 (10 μM) or CsA (1 μM) for the times indicated and incubated with fluoresecent dyes for 15 min at 37°C, and washed with PBS containing 10 mM glucose and analysed immediately by flow cytometry. In each analysis, 10 000 events were recorded.

Laser scanning confocal microscopy. CEM cells were loaded with 1 μM Rhod2-AM in buffer containing 100 mM KCl, 10 mM MOPS pH = 7.2 for 60 min. After loading with Rhod2-AM, cells were transferred to primary culture for an additional 18 h to eliminate the residual cytosolic fraction of the Rhod2 probe. To determine the mitochondrial localization of the Rhod2 probe, cells were simultaneously loaded with 100 nM MitoTracker green (a mitochondria-selective dye which is concentrated by active mitochondria) and 300 nM DAPI in primary culture medium for 60 min. Fluorescence Rhod2 images were acquired using 552 nm excitation and 581 nm emission; fluorescence images of MitoTracker green were acquired using 490 nm excitation and 516 nm emission and DAPI using 358 nm excitation and 461 nm emission as described previously.[36]

Determination of $\Delta_{\Psi m}$. Determination of $\Delta_{\Psi m}$ was performed as described previously.[31] Briefly, cells were loaded with TMRM (250 nM) for 15 min and red fluorescence was determined by FACS analysis using PE setting. In each analysis, 10 000 events were recorded.

Transmission electron microscopy (TEM). CEM cells in the logarithmic proliferation phase were treated with THG (1 μM) ± the inhibitors as described in figure legends. Cells were fixed with 2.5% glutaraldehyde in 0.1 M cacodylate buffer, pH 7.4, at room temperature for 1 h and washed with 0.1 M cacodylate buffer and postfixed with 1% osmium tetroxide in 0.1 M cacodylate buffer and dehydrated with graded series of ethanol, and embedded in LX112. Thin sections were prepared,

Figure 8 Hypothetical model showing key events regulating ER-stress-induced apoptosis in human leukemic CEM cells. The Ca^{2+}-induced MPT and structural changes to the mitochondrial cristae and possibly contact junction (CJ) are responsible for the release of the major fraction of cytochrome *c* from the ETC to activate apoptosis. Bax forms a simple pore or channel in the mitochondrial outer membrane to facilitate the release of cytochrome *c* into the cytosol. In the model we show that Bax and the MPT are independent events activated by ER stress, but cooperate to bring about the complete release of cytochrome *c* from mitochondria leading to caspase 3-dependent apoptosis

Thapsigargin mediated Endoplasmic reticulum stress

Cytosolic Ca²⁺ increase

Mitochondrial calcium overload

Bax targeting to mitochondria

Permeability transition/ cristae remodeling

Non-ETC derived cytochrome c + *ETC-derived cytochrome c*

Caspase-3 dependent apoptosis

and stained with uranyl acetate. Specimens were examined on a JEOL 1000 × electron microscope operating at 80 kV.

Subcellular fractionation. Subcellular fractionation was performed as described previously with the following modifications.[37] Following treatment, cells ($\sim 1 \times 10^7$) were harvested by centrifugation (600 × g for 10 min at 4°C). Cell pellets were washed with ice-cold PBS and suspended in HEPES buffer at pH 7.4. Cells were disrupted using a $27\frac{1}{2}$ gauge needle and the cell homogenate was centrifuged at 800 × g for 10 min at 4°C to remove nuclei and unbroken cells. The supernatant from this preparation was centrifuged at 10 000 × g for 10 min and the pellet was designated the 'mitochondrial' fraction, whereas the supernatant was centrifuged at 100 000 × g for 60 min at 4°C and the resulting supernatant was used for preparation of cytosolic fraction. The mitochondrial and cytosolic fractions were stored at −80°C until experimentation. Protein assay was performed by Dc protein assay (Bio-Rad, Hercules, CA, USA).

Mitochondrial isolation, swelling test and detection of cytochrome *c* release. RLM were isolated by conventional differential centrifugation from the livers of male adult Sprague–Dawley rats fasted overnight.[38] The isolation buffer consisted of mannitol (220 mM), sucrose (70 mM), Hepes (2 mM), EGTA (0.5 mM) and bovine serum albumin (0.1%), pH 7.4. Isolated RLM were suspended in storage buffer consisting of 200 mM sucrose and 2 mM HEPES, pH 7.4. Large amplitude swelling was measured by spectrophotometry in a Beckman DU 640 by recording absorbance change at 540 nm in incubation buffer consisting of 200 mM sucrose, 20 μM EGTA, 5 mM succinate, 2 μM rotenone, 1 μg/ml oligomycin, 20 mM Tris, 20 mM HEPES and 1 mM KH$_2$PO$_4$, pH 7.2. To measure cytochrome *c* release from RLM induced by different additions, RLM (0.5 mg/ml) in storage buffer were incubated with Ca^{2+} (625 μM)+CsA (50 μM) or DIG (100 pmol/mg protein) for 10 min, then the incubated RLM were centrifuged at 10 000 × g for 10 min at 4°C. The supernatant fractions were further spun at 100 000 × g for 15 min at 4°C to eliminate mitochondrial membrane fragments and the resulting supernatants were used to determine cytochrome *c* released from RLM.

Mitochondrial oxygen consumption. Oxygen consumption was measured with a Clark oxygen electrode (Oxygraph Model 5300: Yellow Spring Instrument Co., Yellow Spring, OH, USA) as described previously.[39] Oxygen consumption was monitored in 150 mM sucrose, 5 mM MgCl$_2$, 5 mM succinate, 1 μM, rotenone and 10 mM NaPi buffer, pH 7.4. Respiratory control ratios (RCR) were calculated after addition of 200 μM ADP to initiate state 3 respirations.

Immunoblotting. Proteins were separated by electrophoresis on 14% SDS-PAGE gels and transferred to nitrocellulose membrane. Protein concentration was determined using Bio-Rad Dc protein assay. Rabbit polyclonal anti-Bax (N20) antibody was purchased from Santa Cruz Biotechnology (Santa Cruz, CA, USA), whereas rabbit polyclonal anti-Cyp-D antibody was from Calbiochem (San Diego, CA, USA). Mouse monoclonal anti-cytochrome *c*, anti-β actin and anti-MnSOD antibodies were from BD Biosciences, Pharmingen (San Diego, CA, USA). The secondary antibodies used were goat anti-rabbit and goat anti-mouse horseradish peroxidase-conjugated antibodies, respectively, and they were purchased from BD Biosciences, Pharmingen (San Diego, CA, USA). Chemiluminescence detection was performed using ECL detection kit according to the manufacturer's instructions (Pierce, USA).

Bax and Cyp-D gene silencing with siRNAs. Gene silencing with siRNAs (sense and antisense strands) were purchased from 1st base, Britain. The sense strand sequences were: control, 5′-UUCUCCGAACGUGUCACGU (dTdT)-3′; Bax, 5′-GGUGCCGGAACUGAUCAGA(dTdT)-3′ and Cyp-D, 5′-CCUGCUAAAUUGUGCGUUA(dTdT)-3′. Cells were transfected with siRNAs using lipofectamine 2000 (Invitrogen, CA, USA) according to the manufacturer's instructions for 48 h unless otherwise stated. Following transfection, cells were harvested for experiments as described for parental CEM cells.

Statistical analysis. Data were expressed as standard error of the mean (S.E.) of three or more separate experiments performed in duplicate. ANOVA was used for significance testing ($P < 0.05$).

1. Boyce M, Yuan J. Cellular response to endoplasmic reticulum stress: a matter of life or death. *Cell Death Differ* 2006; **13**: 363–373.
2. Yamaguchi H, Bhalla K, Wang HG. Bax plays a pivotal role in thapsigargin-induced apoptosis of human colon cancer HCT116 cells by controlling Smac/Diablo and Omi/HtrA2 release from mitochondria. *Cancer Res* 2003; **63**: 1483–1489.
3. Yamaguchi H, Wang HG. CHOP is involved in endoplasmic reticulum stress-induced apoptosis by enhancing DR5 expression in human carcinoma cells. *J Biol Chem* 2004; **279**: 45495–45502.
4. Roucou X, Montessuit S, Antonsson B, Martinou JC. Bax oligomerization in mitochondrial membranes requires tBid (caspase-8-cleaved Bid) and a mitochondrial protein. *Biochem J* 2002; **368**: 915–921.
5. Korsmeyer SJ, Wei MC, Saito M, Weiler S, Oh KJ, Schlesinger PH. Pro-apoptotic cascade activates BID, which oligomerizes BAK or BAX into pores that result in the release of cytochrome *c*. *Cell Death Differ* 2000; **7**: 1166–1173.
6. Scorrano L, Korsemeyer SJ. Mechanism of cytochrome *c* release by proapoptotic BCL-2 family members. *Biochem Biophys Res Commun* 2003; **304**: 437–444.
7. Nechushtan A, Smith CL, Hsu YT, Youle RJ. Conformation of the Bax C-terminal region regulates subcellular location and cell death. *EMBO J* 1999; **18**: 2330–2341.
8. Jürgensmeier JM, Xie Z, Deveraux Q, Ellerby L, Bredesen D, Reed JC. Bax directly induces release of cytochrome *c* from isolated mitochondria. *Proc Natl Acad Sci USA* 1998; **95**: 4997–5002.
9. Antonsson B, Montessuit S, Lauper S, Eskes R, Martinou JC. Bax oligomerization is required for channel-forming activity in liposomes and to trigger cytochrome *c* release from mitochondria. *Biochem J* 2000; **345**: 271–278.
10. Iverson SL, Orrenius S. The cardiolipin–cytochrome *c* interaction and the mitochondrial regulation of apoptosis. *Arch Biochem Biophys* 2004; **423**: 37–46.
11. Orrenius S, Zhivotovsky B. Cardiolipin oxidation sets cytochrome *c* free. *Nat Chem Biol* 2005; **1**: 188–189.
12. Scorrano L, Ashiya M, Buttle K, Weiler S, Oakes SA, Mannella CA et al. A distinct pathway remodels mitochondrial cristae and mobilizes cytochrome *c* during apoptosis. *Dev Cell* 2002; **2**: 55–67.
13. Kim TH, Zhao Y, Ding WX, Shin JN, He X, Seo YW et al. Bid–cardiolipin interaction at mitochondrial contact site contributes to mitochondrial cristae reorganization and cytochrome *c* release. *Mol Biol Cell* 2004; **15**: 3061–3072.
14. Yang JC, Cortopassi GA. Induction of the mitochondrial permeability transition causes release of the apoptogenic factor cytochrome *c*. *Free Radic Biol Med* 1998; **24**: 624–631.
15. Bradham CA, Qian T, Streetz K, Trautwein C, Brenner DA, Lemasters JJ. The mitochondrial permeability transition is required for tumor necrosis factor alpha-mediated apoptosis and cytochrome *c* release. *Mol Cell Biol* 1998; **18**: 6353–6364.
16. Nakagawa T, Shimizu S, Watanabe T, Yamaguchi O, Otsu K, Yamagata H et al. Cyclophilin D-dependent mitochondrial permeability transition regulates some necrotic but not apoptotic cell death. *Nature* 2005; **434**: 652–658.
17. Baines CP, Kaiser RA, Purcell NH, Blair NS, Osinska H, Hambleton MA et al. Loss of cyclophilin D reveals a critical role for mitochondrial permeability transition in cell death. *Nature* 2005; **434**: 658–662.
18. Narita M, Shimizu S, Ito T, Chittenden T, Lutz RJ, Matsuda H et al. Bax interacts with the permeability transition pore to induce permeability transition and cytochrome *c* release in isolated mitochondria. *Proc Natl Acad Sci USA* 1998; **95**: 14681–14686.
19. Marzo I, Brenner C, Zamzami N, Jurgensmeier JM, Susin SA, Vieira HL et al. Bax and adenine nucleotide translocator cooperate in the mitochondrial control of apoptosis. *Science* 1998; **281**: 2027–2031.
20. Zamzami N, El Hamel C, Maisse C, Brenner C, Munoz-Pinedo C, Belzacq AS et al. Bid acts on the permeability transition pore complex to induce apoptosis. *Oncogene* 2000; **19**: 6342–6350.
21. Shimizu S, Ide T, Yanagida T, Tsujimoto Y. Electrophysiological study of a novel large pore formed by Bax and the voltage-dependent anion channel that is permeable to cytochrome *c*. *J Biol Chem* 2000; **275**: 12321–12325.
22. Crabtree GR. Calcium, calcineurin, and the control of transcription. *J Biol Chem* 2001; **276**: 2313–2316.
23. Fruman DA, Klee CB, Bierer BE, Burakoff SJ. Calcineurin phosphatase activity in T lymphocytes is inhibited by FK 506 and cyclosporin A. *Proc Natl Acad Sci USA* 1992; **89**: 3686–3690.
24. Moss ML, Palmer RE, Kuzmic P, Dunlap BE, Henzel W, Kofron JL et al. Identification of actin and HSP 70 as cyclosporin A binding proteins by photoaffinity labeling and fluorescence displacement assays. *J Biol Chem* 1992; **267**: 22054–22059.
25. Epand RF, Martinou JC, Fornallaz-Mulhauser M, Hughes DW, Epand RM. The apoptotic protein tBid promotes leakage by altering membrane curvature. *J Biol Chem* 2002; **277**: 32632–32640.
26. Lucken-Ardjomande S, Martinou JC. Newcomers in the process of mitochondrial permeabilization. *J Cell Sci* 2005; **118**: 473–483.

27. De Giorgi F, Lartigue L, Bauer MK, Schubert A, Grimm S, Hanson GT *et al.* The permeability transition pore signals apoptosis by directing Bax translocation and multimerization. *FASEB J* 2002; **16**: 607–609.

28. He L, Lemasters JJ. Regulated and unregulated mitochondrial permeability transition pores: a new paradigm of pore structure and function? *FEBS Lett* 2002; **512**: 1–7.

29. Kowaltowski AJ, Castilho RF, Vercesi AE. Mitochondrial permeability transition and oxidative stress. *FEBS Lett* 2001; **495**: 12–15.

30. Armstrong JS, Jones DP. Glutathione depletion enforces the mitochondrial permeability transition and causes cell death in Bcl-2 overexpressing HL60 cells. *FASEB J* 2002; **16**: 1263–1265.

31. Armstrong JS, Yang H, Duan W, Chua Y, Whiteman M. Cytochrome bc_1 regulates the mitochondrial permeability transition by two distinct pathways. *J Biol Chem* 2004; **279**: 50420–50428.

32. Jungas T, Motta I, Duffieux F, Fanen P, Stoven V, Ojcius DM. Glutathione levels and BAX activation during apoptosis due to oxidative stress in cells expressing wild-type and mutant cystic fibrosis transmembrane conductance regulator. *J Biol Chem* 2002; **277**: 27912–27918.

33. Liu Z, Lu H, Shi H, Du Y, Yu J, Gu S *et al.* PUMA overexpression induces reactive oxygen species generation and proteasome-mediated stathmin degradation in colorectal cancer cells. *Cancer Res* 2005; **65**: 1647–1654.

34. Simon HU, Haj-Yehia A, Levi-Schaffer F. Role of reactive oxygen species (ROS) in apoptosis induction. *Apoptosis* 2000; **5**: 415–418.

35. Ott M, Robertson JD, Gogvadze V, Zhivotovsky B, Orrenius S. Cytochrome *c* release from mitochondria proceeds by a two-step process. *Proc Natl Acad Sci USA* 2002; **99**: 1259–1263.

36. Hajnoczky G, Robb-Gaspers LD, Seitz MB, Thomas AP. Decoding of cytosolic calcium oscillations in the mitochondria. *Cell* 1995; **82**: 415–424.

37. Yang J, Liu X, Bhalla K, Kim CN, Ibrado AM, Cai J *et al.* Prevention of apoptosis by Bcl-2: release of cytochrome *c* from mitochondria blocked. *Science* 1997; **275**: 1129–1132.

38. He L, Lemasters JJ. Heat shock suppresses the permeability transition in rat liver mitochondria. *J Biol Chem* 2003; **278**: 16755–16760.

39. Chua YL, Zhang D, Boelsterli U, Moore PK, Whiteman M, Armstrong JS. Oltipraz-induced phase 2 enzyme response conserved in cells lacking mitochondrial DNA. *Biochem Biophys Res Commun* 2005; **337**: 375–381.